Cement & Concrete Composites 45 (2014) 136–147

Contents lists available at ScienceDirect

Cement & Concrete Composites

journal homepage: www.elsevier.com/locate/cemconcomp

High-volume natural volcanic pozzolan and limestone powder as partial replacements for portland cement in self-compacting and sustainable concrete

K. Celik [a], M.D. Jackson [a], M. Mancio [a,1], C. Meral [a,2], A.-H. Emwas [b], P.K. Mehta [a], P.J.M. Monteiro [a,*]

[a] Department of Civil and Environmental Engineering, University of California, Berkeley, CA 94720, USA
[b] King Abdullah University of Science and Technology, Thuwal 23955-6900, Saudi Arabia

ARTICLE INFO

Article history:
Received 1 October 2012
Received in revised form 3 August 2013
Accepted 10 September 2013
Available online 18 September 2013

Keywords:
Basaltic ash pozzolan
Limestone filler
Self-consolidating concrete
Compressive strength
Chloride migration
Petrographic analysis

ABSTRACT

A laboratory study demonstrates that high volume, 45% by mass replacement of portland cement (OPC) with 30% finely-ground basaltic ash from Saudi Arabia (NP) and 15% limestone powder (LS) produces concrete with good workability, high 28-day compressive strength (39 MPa), excellent one year strength (57 MPa), and very high resistance to chloride penetration. Conventional OPC is produced by intergrinding 95% portland clinker and 5% gypsum, and its clinker factor (CF) thus equals 0.95. With 30% NP and 15% LS portland clinker replacement, the CF of the blended ternary PC equals 0.52 so that 48% CO_2 emissions could be avoided, while enhancing strength development and durability in the resulting self-compacting concrete (SCC). Petrographic and scanning electron microscopy (SEM) investigations of the crushed NP and finely-ground NP in the concretes provide new insights into the heterogeneous fine-scale cementitious hydration products associated with basaltic ash-portland cement reactions.

1. Introduction

Portland cement concrete is the most widely used human-made commodity on the planet; about 25 billion metric tonnes are produced globally each year [1]. About 3.3 billion tonnes of portland cement (OPC) were used in 2010 [2], mainly for concrete construction projects. Concrete domination in construction environments results from its proven flexibility and adaptability, low maintenance requirements during the service life of most structures, and widespread availability of its raw constituents [3]. However, the massive production and consumption cycle of concrete has significant environmental impacts [4]. Global portland cement production currently accounts for 7% (2.1×10^9 tonnes) of anthropogenic carbon dioxide (CO_2) emissions annually, resulting mainly from production of cement clinker, the active binding ingredient of concrete [5]. Because kiln-fired portland cement is an energy-intensive material, requiring 4–5 GJ per ton of cement [4], about half of these emissions occur through combustion of fossil fuels. The remaining emissions result from calcination of limestone: one kg of portland cement clinker releases 0.87 kg of CO_2 to the atmosphere [6]. Increased volume fractions of supplementary cementitious materials (SCM), such as fly ash, slag, and volcanic pozzolans produce more environmentally-sustainable concretes, and also yield mixtures with high workability, ultimate strength, and durability [3].

To eliminate 1 billion tonnes of CO_2 per year through the concrete sector, approximately 50% of the clinker factor (CF) of portland cement must be replaced with materials produced with very low carbon dioxide emissions [7]. This would require 1.58 billion tonnes of alternative SCM annually. High volume fly ash (HVFA) mixtures have been utilized successfully in many projects as a low-cost alternative to conventional portland cement concrete, with proven technical and environmental advantages [8]. However, the global availability of fly ash is about 800 million tonnes annually [9], and not all of it is suitable for use in blended cements, or in concrete mixtures. Recently, natural basaltic ash pozzolan replacement of portland cement at 25 mass%, from Saudi Arabia, has been shown to be a successful alternative [10]. In addition, natural zeolite and volcanic tuff pozzolan replacement of OPC at 50 mass%, from Turkey, and a higher w/c ratio than the present study led to a slow strength gain, but relatively good compressive strength and durability characteristics [11]. Studies of portland cement-based

* Corresponding author. Tel.: +1 510 643 8251; fax: +1 510 643 5264.
E-mail addresses: kcelik@berkeley.edu, ckemal@gmail.com (K. Celik), mdjackson@berkeley.edu, mdjjackson@gmail.com (M.D. Jackson), mancio@gmail.com (M. Mancio), caglameral@gmail.com (C. Meral), abdelhamid.emwas@kaust.edu.sa (A.-H. Emwas), pkmehta@berkeley.edu (P.K. Mehta), monteiro@ce.berkeley.edu (P.J.M. Monteiro).
[1] Present address: Unisinos University, Graduate Program in Civil Engineering (PPGEC), Av. Unisinos, 950, 93022-000 Sao Leopoldo, RS, Brazil.
[2] Present address: Department of Civil Engineering, Middle East Technical University, 06800 Ankara, Turkey.

0958-9465/$ - see front matter © 2013 Elsevier Ltd. All rights reserved.
http://dx.doi.org/10.1016/j.cemconcomp.2013.09.003

ternary and quaternary blends containing combinations of fly ash, silica fume, blast furnace slag, limestone filler and natural volcanic pozzolans show that blended cements can be optimized to minimize the shortcomings of each component, resulting in synergistic cementitious systems [12,13].

This research investigates the mechanical and durability performance of SCC mixtures containing high volume portland cement replacements of finely-ground limestone (LS) and finely-ground basaltic ash (NP) from Harrat Rahat, Jabal Kadaha quarry, Medina Province, Saudi Arabia. Western Saudi Arabia has numerous lava and cinder cone fields in widespread *harrats* (Fig. 1 [14]), produced about 25 Ma ago through continental intraplate volcanism associated with rifting of North East Africa to form the Gulf of Aden and the Red Sea [15]. In the laboratory experiments, we utilize binary OPC-NP mixtures with finely ground 30 mass% and 50 mass% NP (30 NP, 50 NP), and ternary OPC–NP–LS mixtures with 30 NP, 40 NP, and 50NP with or without 15 mass% (15 LS). Although the overall pozzolanicity of the ash has been previously measured [16], the role of individual components has not been specifically evaluated. Here, the crushed cinders are described with petrographic analyses (Fig. 2) to show how an inexpensive, straightforward optical microscopic technique can provide rapid insights into the reactivity of the various components of typical basaltic volcanic ash – volcanic glass, crystal fragments, lava rock fragments, and vesicle surface coatings – and the new cementitious products formed in the resulting concrete. Construction material testing applications then describe the mechanical properties and durability performance of the various blends, and the influence of the LS and NP mixtures in the ternary OPC blends on the strength and durability properties of the concretes is discussed. Petrographic and scanning electron microscopy (SEM) investigations of the 70 OPC–30 NP and 50 OPC–50 NP binary blends provide an initial evaluation of the results of the testing experiments and how compositions of cementitious hydrates vary as a function of pozzolanic reaction of NP components with OPC.

Fig. 1. Schematic map showing the cenozoic lava and cinder cone fields, or *harrats*, of western Saudi Arabia, adapted from [15], and the site of the basaltic ash from Jabal Kadaha, Harrat Rahat used in the experimental concretes.

2. Materials

2.1. Geologic materials used as portland cement replacements

2.1.1. Limestone powder

During the last decade, LS as calcite, or crystalline $CaCO_3$, has proven to be an effective partial replacement for OPC [17]. LS has two functions: it acts as a relatively inert calcareous filler and a limited participant in the hydration process [18–20]. During cement hydration, finely ground $CaCO_3$ reacts with C_3A and C_4AF to form high and low forms of carboaluminates [21]. Calcium hemicarboaluminate forms as an early hydration product in calcite-containing OPC, and then converts nearly completely to calcium monocarboaluminate, a stable AFm phase, after about 28 days [22]. The particle size of LS must be considered in the mix design because the early strength of the concrete depends on blended cement composition and LS fineness, since interaction between gypsum and limestone during early C_3A hydration interferes with setting time [23]. An acceleration of C_3S hydration may occur at early ages when LS is interground with clinker [24]. The catalytic effect results from the high specific surface area of LS, which produces nucleation sites for cement hydration products such as calcium carbosilicate hydrate [25], thus reducing the size of C–S–H agglomerations. In blended cements with up to 5% calcite, for example, almost all of the added calcite reacts with cement [18]. The resulting concretes show compressive strength [26], flexural strength, and drying shrinkage [27] similar to control concretes without LS. At 25% sand mass replacement with LS in mortar specimens, the fine $CaCO_3$ particles produce denser packing of the cement paste and better dispersion of cement grains [28]. When LS replacement of OPC exceeds 15% by mass, however, the less reactive calcite has a dilution effect on the more reactive cement; the amount of cement paste is considerably reduced, resulting in lower compressive strengths and physical modifications [25,29]. Durability decreases as water absorption and chloride diffusion coefficients increase [29].

2.1.2. Basaltic volcanic ash

Volcanic ash pozzolans fall into two major categories: cinder cone eruptions produce scoriae, frothy droplets of molten rock with mainly basaltic compositions, where amorphous glass is usually the predominant reactive component, while more explosive pyroclastic flow eruptions of molten and solid rock fragments produce complex deposits that commonly develop secondary pozzolanic clay and zeolitic surface coatings through interactions with interstitial ground and surface waters [30–33]. The binding pozzolanic mortars of 2000-year-old concretes in the monuments of imperial age Rome, for example, contain 40–50 vol.% scoriaceous volcanic ash from a specific pyroclastic flow with reactive zeolitic and clay mineral surface coatings [33]. Recently, basaltic ash erupted from cinder cones in Saudi Arabia has been used successfully as SCM that complies with the requirements of ASTM C618 for Class N natural pozzolan [14,16,34]. Moufti et al. [16] found that the pozzolanic reactivity of lime with finely-ground cinders from Harrat Khaybar, passing the #200 sieve, satisfies the Italian standard. Khan and Alhozaimy [10] found good effectiveness for up to 25% OPC replacement [16]. The effectiveness of the ash as a larger volume 30–50 mass% OPC replacement has not been evaluated, however, and the reactive components of the ash and associated cementitious products in the resulting concretes have not been described in detail.

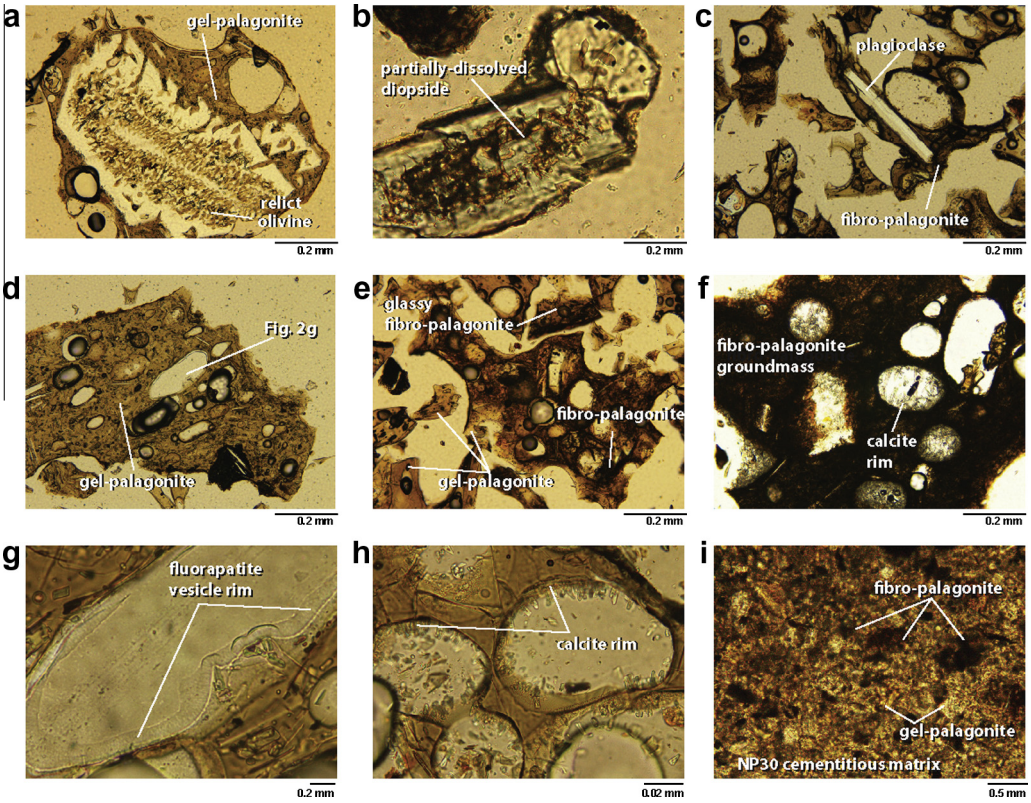

Fig. 2. Petrographic micrographs of Saudi Arabian basaltic ash pozzolan (NP). Survey of volcanic fragments, plane polarized light: (a) dissolved crystal, probably olivine, (b) etched diopside, (c) intact anorthite, (d) gel-palagonitic glass, (e) transition to fibro-palagonitic glass, (f) fibro-palagonitic groundmass of a lava lithic fragment, with calcite surface coatings in vesicles, (g) gel-palagonite glass (Fig. 2d) with fluoroapatite rims on a vesicle surface, (h) gel-palagonite glass with calcite crystals on vesicle surfaces, and (i) cementitious matrix of the 70 OPC–50 NP concrete mix at one year hydration. The dense opaque fabric results from intergrown, amorphous, cementitious hydrates that surround silt to fine sand-sized, partially-reacted gel-palagonite particles. Dark lava lithic fragments with poorly-reactive fibro-palagonite ground mass remain largely intact.

The bulk chemical composition of the Jabal Kadaha NP indicates an alkali basalt (Table 1). Optical micrographs (Fig. 2) from petrographic investigations of crushed sand-sized particles of the basaltic ash, which is similar to other Saudi Arabian *harrat* basalts [10,16,34] provide a qualitative assessment of the various glass and crystal components available for pozzolanic reaction in the experimental concretes. The mineralogical composition determined by X-ray diffraction (Fig. 3a), and confirmed with petrographic observations, indicates a glassy amorphous groundmass, and crystals of plagioclase with an anorthitic composition ($CaAl_2Si_2O_8$), olivine with a forsteritic composition (Mg_2SiO_4), and clinopyroxene with a diopsidic composition ($MgCaSi_2O_6$) (Fig. 2a–c, see [35] for petrographic techniques of mineral identification). Some olivine and diopside crystals have partially dissolved (Fig. 2a–c), and fresh sideromelane glass is generally absent. Rather, the glass has altered to clear, translucent, optically isotropic, gel-palagonite (Fig. 2d), yellowish-olive brown in plane polarized light [36]. This commonly grades into transitional, glassy, fibro-palagonite, which is dark-dusky brown in plane polarized light, with a fine, fibrous, opaque, texture (Fig. 2e). The groundmass of lava rock fragments from the volcanic edifice that were entrained in the magma during eruption to the earth's surface, have a strong fibro-palagonite texture (Fig. 2f).

Resinous, yellow brown gel-palagonite (Fig. 2d) is the most abundant component of the volcanic ash. Palagonite is a stable alteration product of fresh volcanic glass that has interacted with aqueous solutions on or near the earth's surface, and lost Si, Al, Mg, Ca, Na and K, gained H_2O, and become preferentially enriched in Ti and Fe [36]. These trends are further emphasized in fibro-palagonite, which seems to develop very poorly-crystalline clay mineral not detectable through standard X-ray diffraction analyses [36]. The palagonitization process commonly involves the precipitation of secondary phases, mainly crystalline clay minerals, zeolites, or calcite [36], many of which have pozzolanic properties [14,33]. Although subaerial alteration of the volcanic glass of Jabal Kadaha NP produced palagonite, there are only occasional secondary authigenic surface coatings. These are thin rims thin rims of fluoroapatite ($Ca_5(PO_4)_3F$ and calcite on vesicle surfaces (Fig. 2f–h). The precipitation of fluorapatite may reflect the movement of low-temperature waters locally saturated with respect to fluorine and phosphorous through the ash deposit [37], possibly associated with dissolution of apatite-bearing mantle xenoliths in the basaltic ash [38]. Calcite is a common authigenic mineral in basaltic ash and may be associated with CO_2 that combines with calcium in interstitial ground water. These mineral coatings constitute only a minuscule volume of the NP, and are not present in

Table 1
Chemical composition of powder materials (oxides, % by weight).

	OPC	NP	LS
SiO_2	20.44	46.48	0.70
Al_2O_3	3.97	14.74	0.50
Fe_2O_3	4.07	12.16	0.12
CaO	62.9	8.78	47.4
MgO	2.42	8.73	6.80
Na_2O	0.37	3.39	–
K_2O	0.43	1.27	–
P_2O_5	0.16	0.629	–
TiO_2	0.23	2.31	–
MnO	0.32	0.19	–
L.O.I.	4.69	1.324	44.48

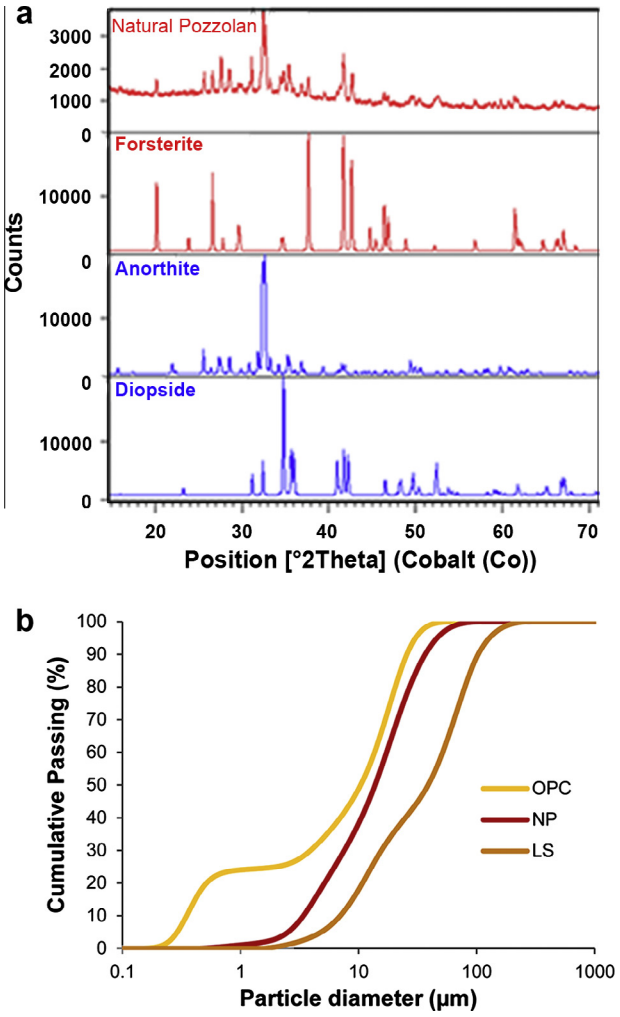

Fig. 3. Chemical and particle size analyses of the powdered cement constituents. (a) X-ray diffraction (XRD) analysis of the Saudi Arabian basaltic volcanic ash from Harrat Rahat used as as a pozzolanic OPC replacement in the laboratory concrete studies, and (b) particle size distribution of OPC, LS, and NP.

sufficient quantities to be detected by the X-ray diffraction analysis (Fig. 3a).

2.2. Blended cements and aggregates

OPC used in this study meets ASTM Type I/II standard specification, and the OPC and NP have mean particle diameters of 10 m and 17 m, respectively (Fig. 3b, Table 2). The mean particle diameter of LS used in the OPC–LS control and OPC–LS–NP ternary blends is 48 m. The fine aggregate (FA) of the concrete mixtures is quartz sand, with 3.1 fineness modulus. The coarse aggregate (CA) consists of 30 mass% pea gravel with maximum size 12.7 mm, containing 70 mass% basaltic coarse aggregate, not from the Saudi source, with maximum size 19.0 mm. A high-efficiency polycarboxylate-based superplasticizer (ADVA-405) with specific gravity of 1.04 kg/l was used as <1.5 mass% cement (Table 3).

3. Experimental and analytical methods

3.1. Concrete mixture proportions

The initial parameters considered for the cement mix design were the proportional aggregate fractions, powder content, and workability (Table 3). The w/cm was held at 0.35 for all mixes; water reducer (SP) was added until the slump flow diameter was between 635 mm and 690 mm; and the flow time was 3–5 s until a diameter of 50 mm, T_{50}, was attained. In order to reduce cement content relative to typical SCCs, the ratio of total aggregates to cementing materials was fixed at 4 to 1, and the total cement replacement ratio ranged from 30 mass% to 65 mass%. For the ternary blends, LS content was set as 15 mass%, and NP varied from 30 to 50 mass% of the total mix. The mix designs are designated 55 OPC–15 LS–30 NP, for example, for the 55 mass% OPC, 15 mass% LS, and 30 mass% NP mix. The ratio of CA to FA was kept at a constant 1:1 mass% ratio. The control mixes contain either 100 OPC–0 LS–0 NP or 85 OPC–15 LS–0 NP as the powder materials.

3.2. Concrete mixing and casting

For each mix, a total volume of 22L (5.81 gallons) of concrete was prepared in a pan planetary-type mixer with the following procedure: the CA and a small amount of water were mixed for 30 s; the OPC, NP, and more water were added and mixed for 1 min; the limestone powder and the rest of the water were added and mixed for 1 min; the water reducer was added and mixed for 1 min. Finally, the FA was then added and mixed for 3 min. During that time, the mixer was stopped and the bottom scraped to remove any fine particles that might have collected at the bottom. The slump flow test was then performed (see Section 3.3). If the concrete was satisfactory, it was returned to the mixer and mixed for an additional minute before casting. If the slump flow was too low or flow time too high, the concrete was returned to the mixer, mixed for an additional minute and additional water reducer added until workability appeared sufficient. The slump flow test was again performed. If the concrete was satisfactory, it was then remixed for an additional minute before casting. Otherwise, it was discarded and the mix attempted again with more or less water reducer. The material was cast into eighteen 75 × 150 mm cylinders and three 100 × 200 mm cylinders in two lifts without mechanical vibration. Light shaking was allowed as the only method of consolidation. The cylinders were immediately covered with plastic wrap and left undisturbed for 24 h at 25 °C in the ambient laboratory environment. The cylinders were then demolded and placed in a fog-room chamber at 100% relative humidity at room temperature, 23 ± 2 °C, to cure until testing in accordance with ASTM C192 [39]. Each mix was then evaluated using slump flow, compressive strength, chloride penetration coefficient, water absorption, and gas permeability testing as basic indicators of workability, mechanical strength, and durability properties.

Table 2
Particle size distribution of OPC, LS and NP used in experimental concretes.

	Mean (µm)	Median (µm)	Mode (µm)	Standard Deviation (µm)	D10 (µm)	D50 (µm)	D90 (µm)
OPC	10.4	11.7	18.5	10.2	0.3	10.4	25.7
LS	48.1	38.7	72.0	41.9	7.0	15.6	38.7
NP	17.4	13.8	18.5	14.5	3.4	13.7	36.8

Table 3
Concrete mix proportions.

	OPC–LS–NP (%)	OPC	NP	LS	FA	CA	W/CM	SP (%)
Control mixes	100–0–0	1.00	–	–	2	2	0.35	1.43[a]
	85–15–0	0.85	–	0.15	2	2	0.35	1.4[a]
Binary HVNP blends	70–0–30	0.70	0.30	–	2	2	0.35	1.08
	50–0–50	0.50	0.50	–	2	2	0.35	1.03
Ternary HVNP-LS blends	55–15–30	0.55	0.30	0.15	2	2	0.35	1.22
	45–15–40	0.45	0.40	0.15	2	2	0.35	1.22
	35–15–50	0.35	0.50	0.15	2	2	0.35	1.12

[a] The chemical admixture used was an entry-level carboxylated polyether-based high-range water reducer (ADVA 140) with a specific gravity of 1.010–1.120.

3.3. Slump flow test

The SCC slump flow test (ASTM C1611) [40] was performed to determine the fresh-state properties of each mix. The flow diameter and T_{50} were verified to be between 635 and 690 mm, and 3–5 s, respectively. In addition, the SCC stability was observed visually by examining the concrete mass in terms of segregation, bleeding, and the mortar halo near the slump flow perimeter.

3.4. Compressive strength test

Compressive strength tests were performed after 7, 28, and 91 days, and at one-year hydration. In accordance with ASTM standards, rubber pads capped the 7-day-old samples; all others were capped with sulfur capping compound. The cylinders were compressed using a displacement rate-based machine until significant softening was observed according to ASTM C39 [41]. The peak load value was taken as the compressive strength. In order to identify and remove outliers from data set, the coefficient of variation (ratio of standard deviation to mean) was kept less than 10% for each mix-curing period combination. The cylinder size was chosen for convenience and economy, even though testing of 75 × 150 mm (3 × 6 in.) cylinders has been shown to underestimate compressive strength by about 102.94%, compared to the standard-sized 100 × 200 mm (4 × 8 in.) cylinder strength of a similar class of concrete produced with a maximum aggregate size of 19.0 mm (¾ in.) [42]. Similar tests [43] indicate that the use of smaller specimens in compressive strength tests may result in lower strengths as compared with standard-size specimens. Therefore, the following equation calculates the correct compressive strength:

$$\sigma'_c = \frac{4P}{\pi d^2} \times 102.94\% \quad (1)$$

where σ'_c is compressive strength, P is magnitude of the load that caused breaking, and d is the diameter of the cylinder.

3.5. Non-steady state chloride migration test

The chloride migration coefficients of the one-year-old concrete samples were determined according to NT BUILD 492 [44], where the test duration and electrical potential were 24 h and 30 V, respectively. After sawing the 100 × 200 mm cylinders into slices, 50 ± 2 mm thick, and brushing and washing away any burrs from the surfaces, the specimens were returned to the fog room until the testing date. The test steps were as follows: (a) the specimens were vacuum soaked with a saturated $Ca(OH)_2$ solution, (b) a 30 V electrical potential was applied that forces chloride ions from a 10% NaCl solution (catholyte) to migrate into the specimen, and (c) the initial current through each specimen was recorded (Fig. 4a). Three specimens were tested for each mix. Each specimen was then split axially into two pieces, and a 0.1 M $AgNO_3$ solution sprayed on the freshly split surfaces. The chloride penetration depth was precisely

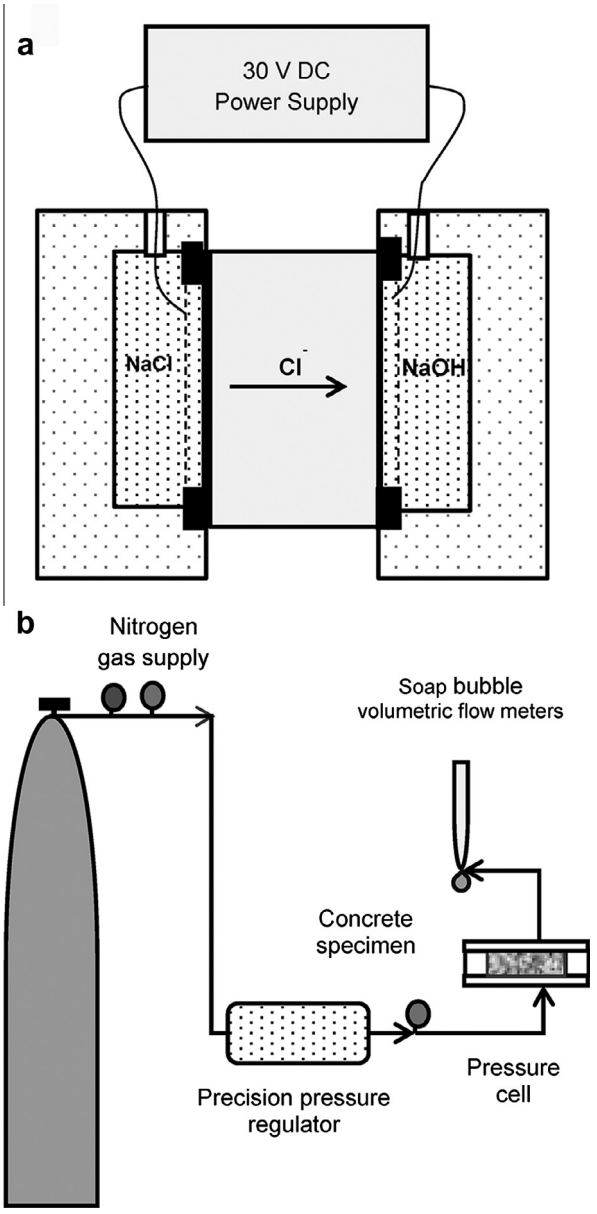

Fig. 4. Schematic diagrams of experimental testing devices. (a) Test set-up of the chloride migration test, and (b) typical setup for the gas permeability test.

measured on photographic images of the specimens enlarged in Adobe Photoshop at seven points over a 70 mm distance from the white silver chloride precipitation. From the mean penetration depth, the non-steady state chloride migration coefficient D_{nssm} (2) was calculated, as described in NT BUILD 492 [44], with:

$$D_{nnsm} = \frac{RT}{zFE} \cdot \frac{x_d - \alpha\sqrt{x_d}}{t} \quad (2)$$

where

$$E = \frac{U-2}{L}$$

and

$$\alpha = 2\sqrt{\frac{RT}{zFE}} \cdot erf^{-1}\left(1 - \frac{2c_d}{c_0}\right)$$

D_{nssm} is the non-steady-state migration coefficient, m^2/s; z is the absolute value of ion valence for chloride, $z = 1$; F is the Faraday constant, 9.648×10^4 J/(V·mol); U is the absolute value of the applied voltage (V); R is the gas constant, 8.314 J/(°K·mol); T is the average value of the initial and final temperatures in the anolyte solution (K); L is the thickness of the specimen (m); x_d is the average value of the penetration depths (m); t is the test duration in seconds; erf^{-1} is the inverse of the error function; c_d is the chloride concentration at which the color of the concrete changes, and generally equals 0.07 N (N is the molar concentration divided by an equivalence factor) for OPC concrete [44]; and c_0 is the chloride concentration in the catholyte solution, about 2 N. Three specimens were tested for each mix, and the average result calculated.

3.6. Water absorption test

The water absorption was determined by immersion on the one-year-old concrete specimens according to the ASTM C948 [45]. First, concrete cylinders 100 mm diameter by 50 mm thick were immersed in approximately 21 °C water and weighed every 24 h, until they attained a mass of less than 0.5% of the heavier saturated surface-dried (SSD) concrete samples; this last SSD mass is designated B. The samples were then oven-dried at 100–110 °C and weighed every 24 h until they attained a mass decrease less than 0.5% of the previously measured weight. The samples were cooled in a vacuum desiccator to room temperature, and weighed, with subsequent dry mass designated as C. The water absorption is calculated as:

$$\text{Water absorption}(\%) = \frac{B-C}{C} \times 100 \quad (3)$$

3.7. Gas permeability test

The gas permeability of the one-year-old concrete specimens was measured with the CEMBUREAU method [46] using nitrogen gas as the permeating medium (Fig. 4b). Five gas pressure stages varying from 0.5 to 2.5 bar (0.05–0.25 MPa) were applied to the dried specimens until the observed weight loss was less than 0.5 g between two successive readings over a time interval of 24 h. Flow times were read every 30 min until a steady-state flow was reached. If the difference between successive readings within 5 min was less than 3%, it was determined that the flow had reached a steady-state condition. For each gas pressure step, the gas permeability coefficient, K_g, was calculated using the Hagen–Poiseuille relationship for laminar flow of a compressible fluid through a porous under steady-state conditions [47], so that:

$$K_g = \frac{2P_0QL_\mu}{A(P^2 - P_a^2)} \quad (4)$$

where K_g is the gas permeability coefficient (m^2); Q is the volume flow rate of the fluid ($m^3\ s^{-1}$); A is the cross-sectional area of the specimen (m^2); L is the thickness of the specimen in the direction of flow (m); μ is the dynamic viscosity of the nitrogen at test temperature (N s m^{-2}); P is the inlet (applied) pressure (absolute) (N m^{-2}); P_a is the outlet pressure assumed in this test to be equal to atmospheric pressure (N m^{-2}); and P_0 is the pressure at which the volume flow rate is determined, assumed in this test to be atmospheric pressure (N m^{-2}).

3.8. Petrographic and scanning electron microscopy investigations

Polished thin sections of the NP and 70 OPC–30 NP and 50 OPC–50 NP concrete mixes with 30% NP and 50% NP replacement of OPC were investigated using optical microscopy techniques and photographed with a Nikon Labophot petrographic microscope. Specific locations of particularly informative microstructures of components of the basaltic ash and associated cementitious hydrates were recorded and then investigated further with an EDAX TSL energy dispersive X-ray spectrometer on the Zeiss EVOMA10 Scanning Electron Microscope (SEM) at the Department of Earth and Planetary Sciences at UC Berkeley. Operating conditions were beam energy of 15 keV, beam current of 850 pA, and counting time of 10 s with 3500 counts per second, reported as relative atomic concentrations.

4. Experimental results and discussion

4.1. Flowability of fresh concrete

According to the slump flow diameter (d_s) and T_{50} results, all mixes produced with the blended cements met specified SCC requirements (Tables 4 and 5 [48]). The visual stability index (VSI) values of the mixes were evaluated between zero and one: zero shows no evidence of segregation or bleeding, and one shows segregation and slight bleeding as a sheen on the concrete mass, in accordance with ASTM C611 [40]. Because of the constant water content but variable use of water reducing agent in the mixes, direct comparisons of the impact of NP and LS replacement on flowability were not possible. However, increasing the amount of NP either decreased the water reducer content and/or T_{50} times, or it increased d_s, indicating that NP has the positive effect of increasing the flowability of the concrete (Table 4). Remarkably, the 100 OPC control concrete had a low flow diameter and high flow times, as compared with the more workable 70 OPC–30 NP concrete, even though the amount of water reducer used in the 100 OPC concrete was 32% larger.

4.2. Compressive strength

Fig. 5 shows that changing the mix proportions of NP and LS has a strong influence on the rate of strength development of the experimental concretes. The binary 70 OPC–30 NP mix results in concrete with only slightly lower strengths compared to the 100 OPC control concrete at all test ages (Fig. 5a). However, the 50 OPC–50 NP mix produced a lower rate of strength development, about 25% less than the control at 1 year. Even so, the 28-day and one-year strength values, 34 MPa and 57 MPa, respectively, are adequate for most structural applications.

Table 4
Slump flow diameter and T_{50}.

OPC–NP–LS (%)	d_s (mm)	T_{50} (s)	SP (%)
100–0–0	584	4.5	1.43
70–30–0	667	3.1	1.08
50–50–0	686	3.8	1.03
85–0–15	622	4.4	1.43
55–30–15	635	4.5	1.22
45–40–15	673	4.5	1.22
35–50–15	648	4.7	1.12

Table 5
Specifications and recommended values for SCC [48].

Workability characteristic	Test methods	Recommended values
Deformability and flow rate (filling ability, unrestricted flow)	Slump flow	Hwang et al. 620 mm to 720 mm EFNARC: 650 mm to 800 mm JSCE: 600 mm to 700 mm PCI: ⩾660 mm Swedish concrete association: 650 mm to 750 mm
	T_{50}	EFNARC: 2–5 s PCI: 3–5 s Swedish concrete association: 3–7 s

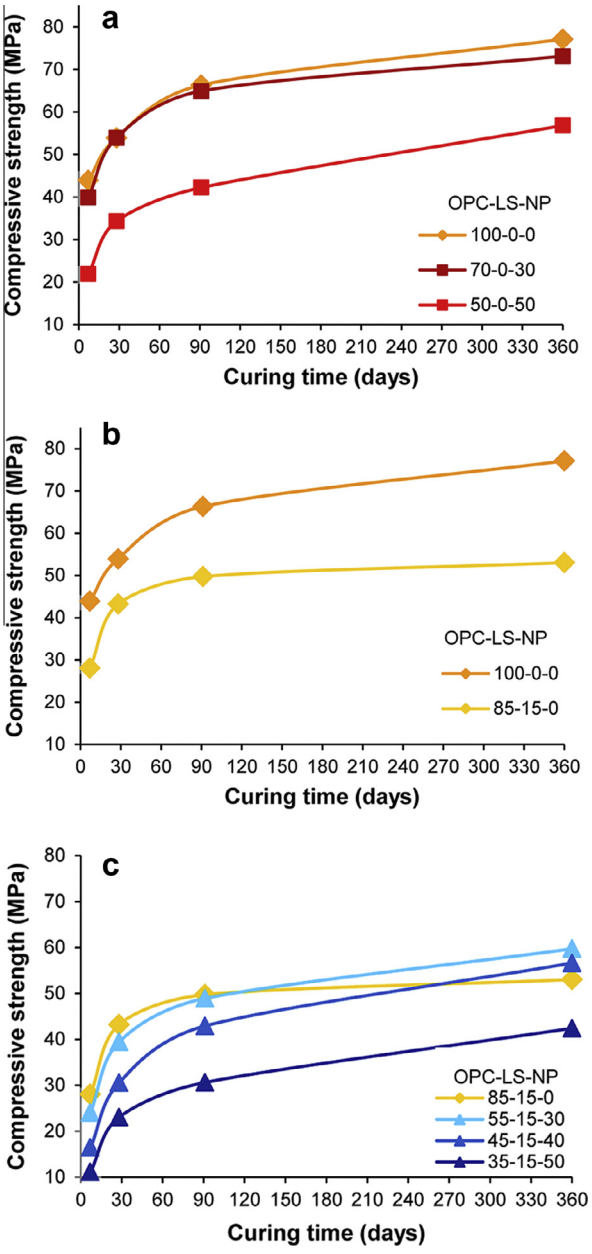

Fig. 5. Results of compressive strength tests of the experimental OPC–LS–NP concretes. (a) OPC–NP binary cement blends, (b) OPC–LS–NP ternary cement blends, (c) OPC and OPC OPC–LS control blends.

The ternary blends with 45–55% OPC replacement contain 15 LS in addition to NP and OPC; they produce concretes with very good long-term compressive strength (Fig. 5c). The 55 OPC–15 LS–30 NP and 45 OPC–15 LS–40 NP concretes show higher long-term strengths than the 85 OPC–15 LS control. At 90 days hydration, for example, the 55 OPC–15 LS–30 NP concrete had compressive strength, 49 MPa, similar to the 85 OPC–15 LS control mix and at one year hydration, the 55 OPC–15 LS–30 NP concrete had a compressive strength, 60 MPa, a bit higher than the control mix, 53 MPa. At 28 days hydration, however, the strengths of 55 OPC–15 LS–30 NP and 35 OPC–15 LS–50 NP concretes were 39 MPa and 23 MPa, respectively. These values are 9% and 47% less than the 85 OPC–15 LS control, and indicate relatively poor performance for the 35 OPC–15 LS–50 NP blend.

Although the 50 OPC–50 NP binary mix showed slightly higher strength, 34 MPa, than the 45 OPC–15 LS–40 NP ternary mix, 30 MPa, at 28 days hydration, both mixes exhibited nearly identical strengths at 90 days and one year hydration, 43 MPa and 57 MPa, respectively. This suggests the large volume ternary mixtures with LS did not interfere with long-term strength development, and that 55% mass replacement of OPC with a finely ground NP–LS mix can be a viable solution to producing SCCs with good long-term strength development. This seems to be the result of adequate pozzolanic activity of NP at up to 40% OPC replacement and a relatively reduced dilution effect of 15% LS replacement of OPC [13,49].

4.3. Durability assessment

4.3.1. Coefficient of chloride migration

The mixing ratio of finely ground NP, and NP–LS as OPC replacement seems to have a strong influence on the chloride migration coefficient of the experimental concretes. All the concretes with blended cement mixes demonstrated a higher resistance to chloride migration relative to the 100 OPC and 85 OPC–15 LS controls. Based on standard guidelines [50], the chloride penetration resistance of the 70 OPC–30 NP binary mix and ternary mixes with a 30NP and 40NP ranges from very high to high (Table 6). The low porosity of Saudi basaltic cinders measured by Sabtan and Shehata [34] may help to reduce the permeability of the resulting concrete. Furthermore, hydration of fine volcanic ash granulates obstructs voids and pores, leading to pore size reduction and smaller effective chloride diffusivity [51]. The 55 OPC–15 LS–30 NP and 45 OPC–15 LS–40 NP mix show very high chloride penetration resistance, while the 50 OPC–50 NP binary mix and the 35 OPC–15 LS–50 NP ternary mix show high resistance to chloride penetration. Concrete with 40 mass% volcanic ash replacement for OPC also shows low chloride ingress [51]. This suggests that both binary NP and ternary NP–LS blends could improve resistance to chloride migration and, possibly, the overall durability and corrosion resistance of the resulting concretes. This could be the result of a pore refinement effect associated with 15% LS replacement of OPC, related to the possible formation of carbo-aluminates and the reduction of ettringite transformation to monosulfate in the ternary mixes [24,12].

Table 6
Resistance against chloride penetration based on non-steady state migration testing [50].

Chloride diffusion D ($\times 10^{-12}$ m^2/s)	Concrete resistance
>15	Low
10–15	Moderate
5–10	High
2.5–5	Very high
<2.5	Extremely high

4.3.2. Water absorption

Variations in the cement replacement mixtures also influence the water absorption of the experimental concretes (Fig. 6b). For both the binary and ternary blends with <50 OPC replacement, water absorption is less than to the 100 OPC and 85 OPC–15 LS controls. This may, perhaps, reflect lower overall porosity. At 55–65 OPC replacement, water absorption is greater than the controls, but at only 2.5–3.5 mass% it is still within acceptable limits. Water absorption describes a material's ability to take in water as a consequence of capillary suction, which is a function of size, distribution, shape, tortuosity, and continuity of its pores [52]. More than 55% OPC replacement in the ternary mixes may induce an increased capillary porosity. This could be attributed to higher water absorption capacity associated with the vesicles of the basalt ash [34], and also the dilution effect of the LS on OPC hydration [23].

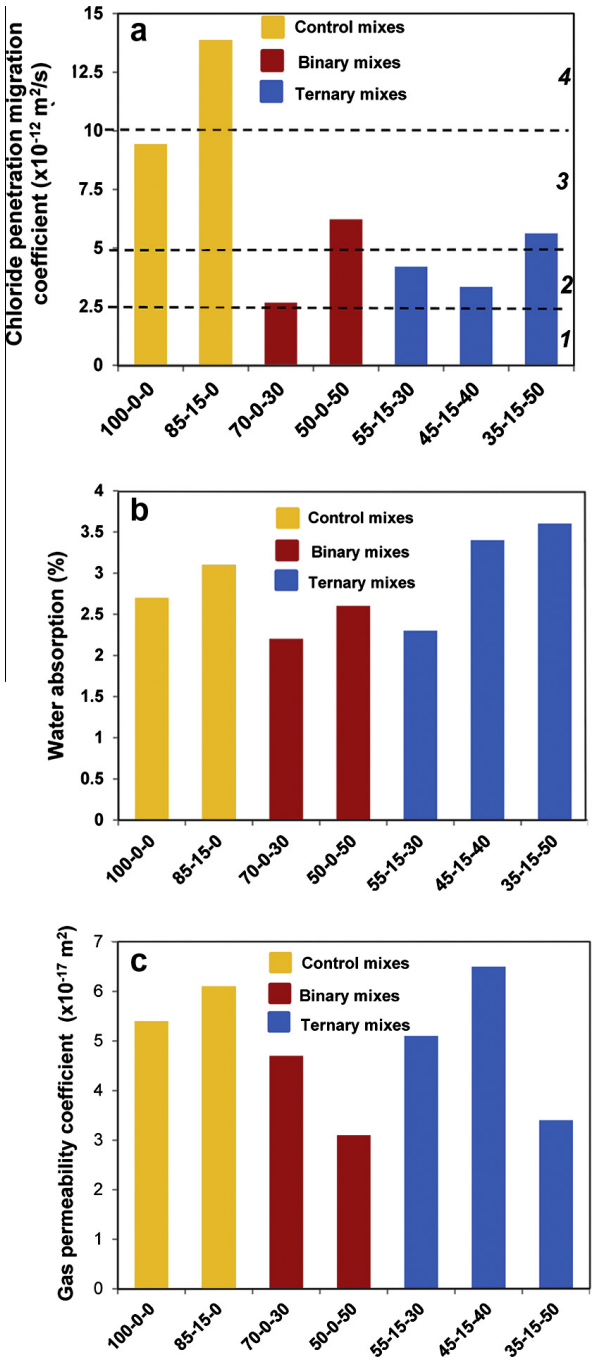

Fig. 6. Results of durability tests of the experimental OPC–LS–NP concretes. (a) Non-steady state chloride migration coefficient as a function of cement replacement of the concrete mix. Zones *1*, *2*, *3* and *4* indicate extremely high to moderate resistance to chloride penetration (Table 6), (b) relationship between water absorption and cement replacement, and (c) gas permeability coefficient in function of cement replacement of the concrete mix. All ratios listed as mass% OPC: LS: NP.

4.3.3. Gas permeability

Variations in the NP and NP–LS mix proportion seem to influence the coefficient of gas permeability in the experimental concretes (Fig. 6c). The greater the amount of OPC replacement with NP, the lower the apparent gas permeability in both the binary and ternary cement systems, with the exception of the 45 OPC–15 LS–40 NP specimens. These appear to be anomalous tests, which could have developed microcracks during the drying process; they have good compressive strength and low chloride penetration.

Adding LS may increase the gas permeability, as shown by the 85–15–0 control mix, but this does not seem have a systematic effect. Although a correlation has been observed between resistance to chloride penetration and decreased gas permeability of concrete subjected to short-term air or oven drying, this effect weakens with longer drying periods [53–57]. This is demonstrated for the specimens tested here at one year hydration: increasing NP replacement of OPC in the binary and ternary mixes generally decreases gas permeability, and it also increases the chloride penetration coefficient, which is the more straightforward measurement. The apparently reduced drying shrinkage of the concrete with increased NP may be related to the refinement of pores through pozzolanic reaction, which obstructs water evaporation [58], and also a higher amount of unreacted ash, which could act as aggregate that restrains shrinkage [59].

4.4. Microscopic investigations of cementitious hydration products

The dense opaque cementitious matrix of the 70 OPC–30 NP concrete mix at one year hydration (Fig. 2i) results from amorphous cementitious hydrates that surround partially-reacted NP particles (Fig. 2d). Lava rock particles of NP generally remain dark and intact, suggesting that their fibro-palagonite ground mass (Fig. 2f) has less pozzolanic reactivity with OPC than the gel-palagonite. The cementitious matrix of the 50 OPC–50 NP concrete mix contains a qualitatively greater proportion of unreacted gel- and fibro-palagonite particles than the 70 OPC–30 NP mix, suggesting that the overall proportion of NP might be too high to produce optimal reaction with OPC and bonding, even after one year hydration. The 50 OPC–50 NP concrete has lower compressive strength, higher water absorption, and greater chloride penetration compared with the 70 OPC–30 NP concrete.

Surface coatings of fluoroapatite, or calcium fluorophosphate ($Ca_5(PO_4)_3F$), in vesicles of the gel-palagonite particles (Fig. 2) could possibly have had a positive influence on binding. Experimental tests of C_3S and C_3A hydration processes indicate that a phosphorous (P_2O_5) and fluorine (F^-) soaking solution reduced early exothermic heat release, and in small concentrations produced an interconnected and compact microstructure in C_3A cementitious hydrates, and a uniform and fine-grained microstructure in C_3S hydrates [60]. Secondary fluoroapatite is common in basaltic cinder deposits [37,38], and easily identified with petrographic analysis in thin section even when not detectable through X-ray diffraction analyses.

Fig. 7 gives examples of how cementitious hydrate compositions vary with proximity to the relicts of gel-palagonite in the 70 OPC–30 NP concrete at the micrometer scale. The OPC bulk composition has calcium in much greater abundance than the

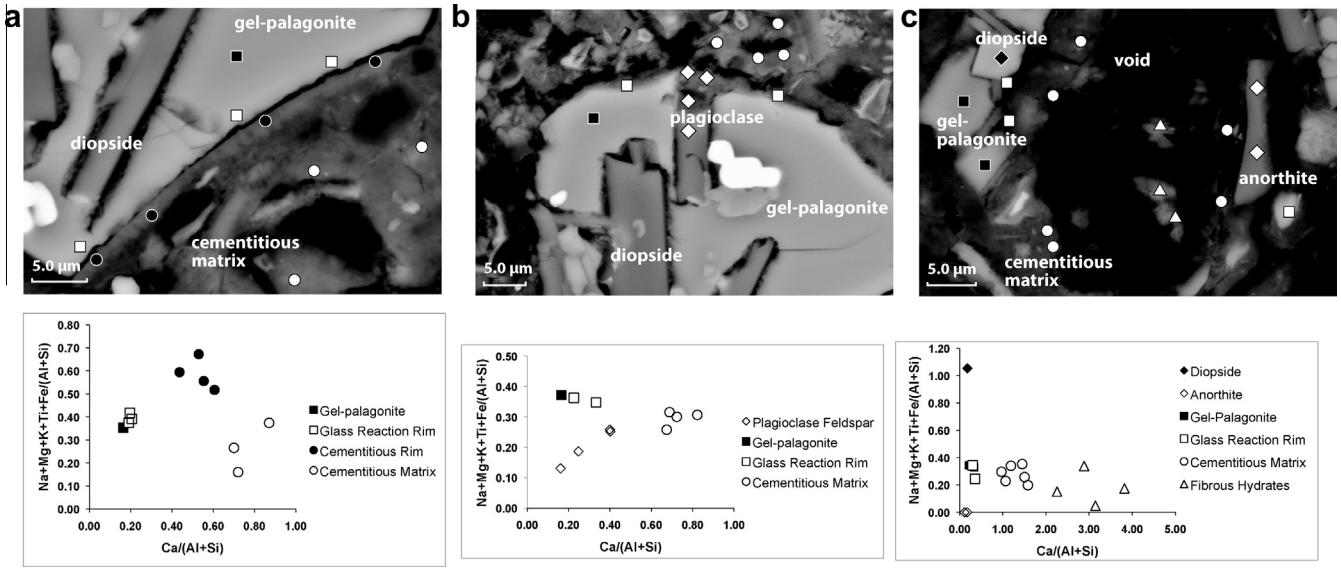

Fig. 7. Reactive components of the basaltic ash and associated cementitious hydrates. Scanning electronic microscope, back-scattered electron images of basaltic ash-OPC reaction products, 5 µm scale bar.

basaltic ash, 62.9 vs. 8.9 mass% CaO, respectively; the NP bulk composition has MgO, Na_2O, K_2O, TiO_2, and FeO_2 in far greated abundance than OPC (Table 1, Fig. 8). Ratios of these cation abundances relative to aluminum and silicon measured in SEM–EDS analyses are plotted in atomic ratio scatter diagrams to provide qualitative illustrations of the incorporation of the chemical species of gel-palagonite in the cementitious binding phase. For example, the coarse silt-sized ash particle of Fig. 7a has gel-palagonite groundmass and reaction rim with moderate Na + Mg + K + Ti + Fe/(Al + Si) = 0.4 and low Ca/(Al + Si) = 0.2, while the cementitious hydrates in the interfacial transition zone have higher Na + Mg + K + Ti + Fe/(Al + Si) = 0.6–0.7, and moderate Ca/(Al + Si) = 0.4–0.6. These compositions seem to reflect close interaction of the neighboring gel-palagonite with OPC pore solutions and incorporation of the dissolved species in alkali-rich cementitious hydrates. In contrast, cementitious hydrates 6–12 m distant from the gel-palagonite have variable Na + Mg + K + Ti + Fe/(Al + Si) = 0.25–0.40 and higher Ca/(Al + Si) = 0.70–0.90, suggesting closer interaction with calcium-rich OPC pore solutions. Plagioclase feldspar in the same particle also reacts with OPC, to form hydrates with lower Na + Mg + K + Ti + Fe/(Al + Si) = 0.20–0.25 and Ca/(Al + Si) = 0.25–0.40 (Fig. 7b). The poorly crystalline calcium–aluminum–silicate hydrate (C–A–S–H) in the cementitious matrix 2–5 m distant has moderate Na + Mg + K + Ti + Fe/(Al + Si) = 0.25–0.35, and higher Ca/(Al + Si) = 0.70–0.85, which seems to reflect closer interaction with calcium-rich OPC pore solutions. Fibrous clusters in open pores (Fig. 7c) have higher Na + Mg + K + Ti + Fe/(Al + Si) = 0.6, and Ca/(Al + Si) = 2.15–3.7, compared with C–A–S–H in the nearby cementitious matrix. These unusual compositions may reflect relict cement grains that may have partially hydrated in alkaline pore fluids with high Na, Mg, Ti, and Fe derived from NP.

Pozzolanic reaction is predominantly an attack on the SiO_2 or Al_2O_3–SiO_2 framework of a reactive material by OH-ions, so that silicate and other anions detach from the framework, and either remain in place or pass into solution [30,61]. The early-formed, *in situ* product is likely to have K^+ and Na^+ as the predominant cations. Al^{+3} substitutes for Si^{+4} in tetrahedral sites, so C–A–S–H with low Ca/Si can absorb more Na^+ and K^+ in interlayer sites due to a valence compensation mechanism as well as increased silanol binding capacity [62]. The alkali-enriched cementitious products in the transition zone of Fig. 7a thus provide an indication that the palagonitic glass is decomposing and releasing cations through pozzolanic reaction with OPC to form alkali-rich C–A–S–H. Farther from the pozzolanic glass, C–A–S–H in the cementitious matrix shows a range of compositions, for example, Ca/(Al + Si) = 0.70–0.90 adjacent to pozzolanic glass (Fig. 7a and b), and Ca/(Al + Si) = 1.0–1.5 adjacent to a relict pore (Fig. 7c).

Fig. 8a summarizes the heterogeneous compositions of the Jabal Kadaha NP components and binding cementitious products in the 70 OPC–30 NP and 50 OPC–50 NP concretes at one year hydration. Unreacted volcanic ash components have Ca/Si < 0.5, and Na + Mg + K + Ti + Fe cation concentrations that reflect gel-palagonite, fibro-palagonite, and diopside and plagioclase crystal compositions (Fig. 8a). The compositions of gel-palagonite reaction rims and interfacial transition zones vary from about Na + Mg + K + Ti + Fe/(Al + Si) = 0.2–0.7 and Ca/Si = 0.2–0.8. This may reflect heterogeneous depletion of the gel-palagonite and local alkali enrichment in cementitious hydrates associated with pozzolanic reaction. The plot of Si/Ca and Al/Mg atomic ratios (Fig. 8b) shows that there are no measurements of cementitious hydrate compositions that fall in the range of hydrotalcite compositions, Al/Mg = 0.23–0.52, common in slag cement pastes [61]. Rather, the compositions seem to correspond to C–A–S–H with Al/Mg = 1–5, Si/Ca = 0.6–1.5 and Al/Ca = 0.1–0.4 (Fig. 8b and c), roughly similar to aluminous C–S–H associated with slag cements [61]. Previous research has shown that adding aluminosilicate pozzolan to OPC lowers the mean Ca/Si ratio of C–S–H gel substantially below its typical value, about 1.7 [62]. Indeed, C–A–S–H in the cementitious matrix of the 50 OPC–50 NP concrete mainly has lower Ca/(Al + Si) = 0.6–1.0 than the 70 OPC–30 NP concrete, with Ca/(Al + Si) = 0.8–1.9 (Fig. 8a). This suggests that a lower proportion of OPC leads to lower calcium concentrations overall. Alkali-cation concentrations in C–A–S–H range from about 0.2–0.5 (Fig. 8a); these seem to be a function of proximity to gel-palagonite (Fig. 7). C–A–S–H associated with the diverse reactive components of scoriacous volcanic ash in the monuments of ancient Rome and glassy pumiceous ash in ancient Roman seawater concretes, for example, also has a range of compositions [63,64]. Laboratory experiments [62], have shown that the presence of Al enhances alkali binding in C–A–S–H, and inhomogeneous alkali sorption likely occurs in

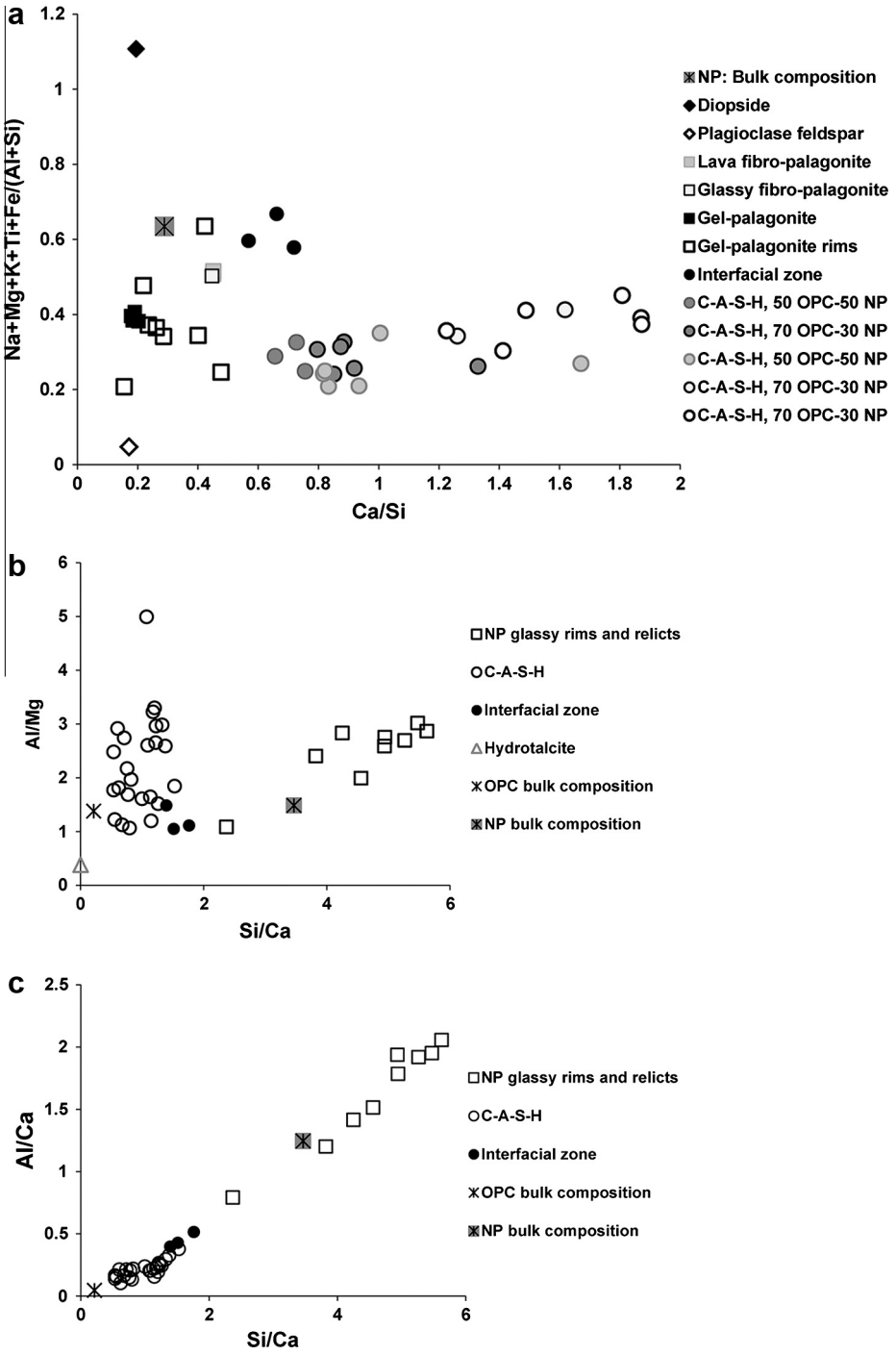

Fig. 8. Compositional overview of the basaltic pozzolan and associated cementitious hydrates showing examples of (a) cation abundances and Ca/Si of the diverse components of NP, and the C–A–S–H binding phase, (b) Si/Ca and Al/Ca of NP gel-palagonite and the C–A–S–H binding phase, (c) Si/Ca and Al/Mg of NP gel-palagonite and the C–A–S–H binding phase. See Table 1 for XRF analyses of NP and OPC, calculated here as elemental percent. All other values are atomic ratios measured from SEM–EDS analyses as Na + Mg + Al + Si + S + P + K + Ca + Ti + Fe.

small clusters of C–A–S–H with low Ca/Si compositions similar to those observed here.

The long-term strength of concretes fabricated with volcanic pozzolans presumably occurs through ongoing reaction of the volcanic ash in the presence of moisture to produce cementitious hydrates, long after OPC is consumed [30,3]. In moist geologic environments gel-palagonite, the principal pozzolanic component of Jabal Kadaha NP (Figs. 1 and 7), commonly reacts with ground and surface waters to produce natural zeolite mineral cements, which bind loose volcanic ash into a coherent rock called tuff [36]. A well-known example of this is the Tufo Lionato palagonitic tuff building stone of Rome, which developed natural zeolite cements within a mid-Pleistocene, and is the predominant decimeter-sized aggregate of the highly durable composite concretes of imperial age Roman monuments [63,65]. Although the gel-palagonite of Jabal Kadaha cinder cone did not develop zeolitic alteration products in the arid environment of western Saudi Arabia, it is conceivable that in a humid concrete environment

the gel-palagonite pozzolan could eventually produce secondary zeolitic cementitious hydrates. Ancient Roman pozzolanic harbor concretes, for example, developed zeolites in the pores of a pumiceous mortar while submerged in seawater [64]. Basaltic cinder cone fields occur throughout the world and their gel-palagonite component, detected through the petrographic analyses described in this study, could play an important role in enhancing the very long-term chemical and mechanical durability of environmentally-sustainable concretes, while substantially reducing CO_2 emissions associated with kiln-fired OPC.

5. Conclusions

Finely-ground natural basaltic ash pozzolan with or without finely-ground LS provides an effective high volume substitute for up to 50% by mass OPC in experimental concretes with good workability, which satisfy self-compacting concrete criteria without costly viscosity-modifying admixtures. Petrographic and scanning electron microscopy studies of the crushed unreacted basaltic ash and 70 OPC–30 NP and 50 OPC–50 NP concretes indicate that resinous, yellow–brown gel-palagonite is the predominant pozzolanic component. Cementitious hydrates in the interfacial zone along the rims of gel-palagonite particles have Ca/(Al + Si) = 0.4–0.6 and Na + Mg + K + Ti + Fe/(Al + Si) = 0.6–0.7, which reflect the lower calcium and higher alkali concentrations of the reacting basaltic glass relative to OPC. The composition of C–A–S–H in the binding cementitious matrix vary from Ca/(Al + Si) = 0.70–1.9, which seem to reflect relative proximity to partially reacted gel-palagonite particles and the overall proportion of NP in the cement mix. A 70 OPC–30 NP binary blend produced 28 day and later strengths of 54–73 MPa, similar to the 100 OPC control; the 50 OPC–50 NP blend shows far lower strengths, 34–57 MPa, perhaps because the cementitious matrix contains a greater proportion of anhydrous phases, including unreacted NP grains. At 28 days, this mix showed higher strength than the 45 OPC–15 LS–40 NP ternary mix, suggesting that the ternary system requires more time to develop cohesion in the hydrated cement paste than the binary system; both mixes had similar strengths at strengths at 90 days and one year, 43 MPa and 57 MPa, respectively. The performance of the 50 OPC–50 NP mix with basaltic ash pozzolan is quite similar to concretes blended with 50 mass% natural zeolite or volcanic tuff replacement of OPC [11], in terms of both early and ultimate strength at 180 days hydration.

The use of 15 mass% LS particles with 48 m median diameter produced lower strength at early and ultimate ages in both the binary and ternary mixes relative to the pure OPC control. A similar study [20] demonstrated that the replacement of 10 mass% OPC by LS with a fine (16 μm median diameter) and a coarse (80 μm median diameter) particle size in binary mixes with w/c of 0.35 also produced lower strength. In comparison, intergrinding portland clinker and limestone generates a finer LS particle size [66]. The resulting binary mortar mix with 10 and 20 mass% LS replacement also had slightly lower strength than that of an OPC control at 7 days and 28 days. This suggests that incorporation of LS leads to slightly lower strength, overall.

All the binary and ternary blend mixes produced higher resistance to chloride penetration than the 100 OPC and 85 OPC–15 LS reference mixes, as has been shown for many blended pozzolanic concretes [51,12,67]. This may be related to pore refinement through pozzolanic cementitious processes and the latent hydraulic properties of NP and LS [61]. Greater than 55% OPC replacement in the ternary mixes resulted in higher water absorption. This could be associated with a higher volume of capillary voids, related to the vesicularity and higher water absorption capacity of the basaltic ash, coupled with the dilution effect of LS and unreacted NP on cementitious processes associated with OPC hydration.

Overall, the 55 OPC–15 LS–30 NP blend produces a low-cost and environment-friendly concrete that does not require calcining of NP or LS with OPC and would reduce CO_2 emissions 48% compared with the 100 OPC control, while providing higher ultimate strength and resistance to chloride penetration, and an aluminous cementitious system associated with basaltic glass-OPC reactions.

Acknowledgements

We thank Super Burkani Blocks for providing crushed and finely-ground basaltic volcanic ash. This research was funded in part by Award No. KUS-l1-004021, from King Abdullah University of Science and Technology (KAUST). Mr. Timothy Teague provided valuable laboratory assistance.

References

[1] WBCSD. The cement sustainability initiative: recycling concrete. In: Klee H, editor. Geneva (Switzerland): World Council for Sustainable Business Development; 2009. p. 1–42.
[2] U.S. Department of the Interior USGS. Mineral commodity summaries 2011. Reston, Virginia: U.S. Geological Survey; 2011.
[3] Mehta PK, Monteiro PJM. Concrete microstructure, properties, and materials. Berkeley: McGraw-Hill; 2006.
[4] Mehta PK. Reducing the environmental impact of concrete. Concr Int 2001:61–6.
[5] IEA-WBCSD, Cement Technology Roadmap 2009 – Carbon emissions reductions up to 2050; 2009.
[6] WBCSD-CSI, Cement Industry Energy and CO_2 Performance "Getting the Numbers Right". Washington, DC; 2009.
[7] Tomkins CD. Redefining what's possible for clean energy by 2020. San Francisco: Gigaton Throwdown; 2009.
[8] Malhotra VM, Mehta PK. High-performance high-volume fly ash concrete for building sustainable & durable structures. 3rd ed. Ottowa (Canada): Supplementary Cementing Materials for Sustainable Development Inc.; 2008.
[9] Mehta PK. Sustainable cements and concrete for the climate change era – a review. In: Zachar PC, Naik TR, Ganjian E, editors. Second international conference on sustainable construction materials and technologies. Italy: Coventry University and The University of Wisconsin Milwaukee Centre for By-products Utilization; 2010.
[10] Khan MI, Alhozaimy AM. Properties of natural pozzolan and its potential utilization in environmental friendly concrete. Can J Civ Eng 2011;38(1):71–8.
[11] Uzal B, Turanli L, Mehta PK. High-volume natural pozzolan concrete for structural applications. ACI Mater J 2007;104:535–8.
[12] Pipilikaki P, Katsioti M. Study of the hydration process of quaternary blended cements and durability of the produced mortars and concretes. Constr Build Mater 2009;23(6):2246–50.
[13] De Weerdt K, Kjellsen KO, Sellevold E, Justnes H. Synergy between fly ash and limestone powder in ternary cements. Cem Concr Compos 2011;33(1):30–8.
[14] Roobol MJ, Pint JJ, Al-Shanti MA, Al-Juaid AJ, Al-Amoudi SA, Pint S. Preliminary survey for lava-tube caves on Harrat Kishb, Kingdom of Saudi Arabia. Jeddah (Kingdom of Saudi Arabia): Saudi Geological Survey; 2002. p. 1–46.
[15] Pallister JS, McCausland WA, Jonsson S, Lu Z, Zahran HM, Hadidy SE, et al. Broad accommodation of rift-related extension recorded by dyke intrusion in Saudi Arabia. Nat Geosci 2010;3(10):705–12.
[16] Moufti MR, Sabtan AA, El-Mahdy OR, Shehata WM. Assessment of the industrial utilization of scoria materials in central Harrat Rahat, Saudi Arabia. Eng Geol 2000;57(3–4):155–62.
[17] Tennis PD, Thomas MDA, Weiss WJ. State-of-the-art report on use of limestone in cements at levels of up to 15%. Portland Cem Assoc 2011:10–20.
[18] Matschei T, Lothenbach B, Glasser FP. The role of calcium carbonate in cement hydration. Cem Concr Res 2007;37(4):551–8.
[19] Poppe A-M, De Schutter G. Cement hydration in the presence of high filler contents. Cem Concr Res 2005;35(12):2290–9.
[20] Bentz DP, Irassar EF, Bucher BE, Weiss WJ. Limestone fillers conserve cement Part 2: Durability issues and the effects of limestone fineness on mixtures. Concr Int 2009(12):35–9.
[21] Hooton RD, Nokken M, Thomas MDA. Portland-limestone cement: state-of-the-art report and gap analysis for CSA A 3000. Ontairo: University of Toronto; 2007.
[22] Ipavec A, Gabrovšek R, Vuk T, Kaučič V, Maček J, Meden A. Carboaluminate phases formation during the hydration of calcite-containing portland cement. J Am Ceram Soc 2011;94(4):1238–42.
[23] Hawkins P, Tennis P, Detwiler R. The use of limestone in portland cement – a state-of-the-art review. Skokie, Illinois (USA): Portland Cement Association; 2003.
[24] Kakali G, Tsivilis S, Aggeli E, Bati M. Hydration products of C3A, C3S and Portland cement in the presence of $CaCO_3$. Cem Concr Res 2000;30(7):1073–7.
[25] Péra J, Husson S, Guilhot B. Influence of finely ground limestone on cement hydration. Cem Concr Compos 1999;21(2):99–105.

[26] Bonavetti V, Donza H, Menéndez G, Cabrera O, Irassar EF. Limestone filler cement in low w/c concrete: a rational use of energy. Cem Concr Res 2003;33(6):865–71.
[27] Lothenbach B, Le Saout G, Gallucci E, Scrivener K. Influence of limestone on the hydration of Portland cements. Cem Concr Res 2008;38(6):848–60.
[28] Benachour Y, Davy CA, Skoczylas F, Houari H. Effect of a high calcite filler addition upon microstructural, mechanical, shrinkage and transport properties of a mortar. Cem Concr Res 2008;38(6):727–36.
[29] Dhir R, Limbachiya M, McCarthy M, Chaipanich A. Evaluation of Portland limestone cements for use in concrete construction. Mater Struct 2007;40(5):459–73.
[30] Massazza F. Pozzolana and pozzolanic cements. In: Hewlett PC, editor. Lea's chemistry of cement and concrete. London: Elsevier Ltd.; 1998. p. 471–632.
[31] Habert G, Choupay N, Montel J, Guillaume D, Escadeillas G. Effects of the secondary minerals of the natural pozzolans on their pozzolanic activity. Cem Concr Res 2008;38(7):963–75.
[32] Snelling R, Mertens G, Elsen J. Supplementary cementitious materials. Rev Miner Geochem 2012;74:211–78.
[33] Jackson M, Deocampo D, Marra F, Scheetz B. Mid-Pleistocene pozzolanic volcanic ash in ancient Roman concretes. Geoarchaeology 2010;25(1):36–74.
[34] Sabtan AA, Shehata WM. Evaluation of engineering properties of scoria in central Harrat Rahat, Saudi Arabia. Bull Eng Geol Environ 2000;59(3):219–25.
[35] Wenk H-R, Bulakh AG. Minerals, their Constitution and Origin. Cambridge: Cambridge University Press; 2009.
[36] Stroncik N, Schmincke H-U. Palagonite – a review. Int J Earth Sci 2002;91(4):680–97.
[37] Gıslason SR, Snorrason Á, Kristmannsdóttir HK, Sveinbjörnsdóttir ÁE, Torsander P, Ólafsson J, et al. Effects of volcanic eruptions on the CO_2 content of the atmosphere and the oceans: the 1996 eruption and flood within the Vatnajökull Glacier, Iceland. Chem Geol 2002;190(1-4):181–205.
[38] Exley RA, Smith JV. The role of apatite in mantle enrichment processes and in the petrogenesis of some alkali basalt suites. Geochim Cosmochim Acta 1982;46(8):1375–84.
[39] ASTM. C192/C192M-07 standard practice for making and curing concrete test specimens in the laboratory1. Safety precautions, manual of aggregate and concrete testing. Annual Book of ASTM Standards, ASTM; 2007. p. 1–8.
[40] ASTM. C1611/C1611M-09b standard test method for slump flow of self-consolidating concrete. ASTM; 2009. p. 1–6.
[41] ASTM. C39/C39M-10 standard test method for compressive strength of cylindrical concrete specimens. ASTM; 2010.
[42] Yousiff AA, Issa MA, Islam MS, Issa SA. Specimen and aggregate size effect on concrete compressive strength. ASTM Intl 2000;22(2):103–15.
[43] Tokyay M, Ozdemir M. Specimen shape and size effect on the compressive strength of higher strength concrete. Cem Concr Res 1997;27(8):1281–9.
[44] NORDTEST. NT BUILD 492: Concrete, mortar and cement-based repair materials: chloride migration coefficient from non-steady-state migration experiments. Finland: Nordtest; 1999. p. 1–8.
[45] ASTM. C948-81 Standard test method for dry and wet bulk density, water absorption, and apparent porosity of thin sections of glass-fiber reinforced concrete. 2009. p. 1–2.
[46] RILEM. RILEM TC 116-PCD:Permeability of Concrete as a Criterion of its Durability_Test for Gas Permeability of Concrete.pdf>. Mater Struct 1999;32:174–9.
[47] Kollek JJ. The determination of the permeability of concrete to oxygen by the Cembureau method – a recommendation. Mater Struct 1989;22:225–30.
[48] Hwang SD, Khayat KH, Bonneau O. Performance-based specifications of self-consolidating concrete used in structural applications. ACI Mater J 2006;103(2):121–9.
[49] Menéndez G, Bonavetti V, Irassar EF. Strength development of ternary blended cement with limestone filler and blast-furnace slag. Cem Concr Compos 2003;25(1):61–7.
[50] Gjørv OE. Durability Design of Concrete Structures in Severe Environments. New York: Taylor & Francis; 2009.
[51] Hossain KMA, Lachemi M. Corrosion resistance and chloride diffusivity of volcanic ash blended cement mortar. Cem Concr Res 2004;34(4):695–702.
[52] Tsivilis S, Tsantilas J, Kakali G, Chaniotakis E, Sakellariou A. The permeability of Portland limestone cement concrete. Cem Concr Res 2003;33(9):1465–71.
[53] Sugiyama T, Bremner TW, Tsuji Y. Determination of chloride diffusion coefficient and gas permeability of concrete and their relationship. Cem Concr Res 1996;26(5):781–90.
[54] Hassan KE, Cabrera JG, Maliehe RS. The effect of mineral admixtures on the properties of high-performance concrete. Cem Concr Compos 2000;22:267–71.
[55] Abbas A, Carcasses M, Ollivier JP. The importance of gas permeability in addition to the compressive strength of concrete. Mag Concr Res 2000;52(1):1–6.
[56] Abbas A, Carcasses M, Ollivier JP. Gas permeability of concrete in relation to its degree of saturation. Mater Struct 1999;32:3–8.
[57] Sugiyama T, Bremner TW, Holm TA. Effect of stress on gas permeability in concrete. ACI Mater J 1996;93(5):443–50.
[58] Itim A, Ezziane K, Kadri E-H. Compressive strength and shrinkage of mortar containing various amounts of mineral additions. Constr Build Mater 2011;25(8):3603–9.
[59] Atiş C. High-volume fly ash concrete with high strength and low drying shrinkage. J Mater Civ Eng 2003;15(2):153–6.
[60] Guo C, Zhu J, Zhou W, Sun Z, Chen W. Effect of phosphorus and fluorine on hydration process of tricalcium silicate and tricalcium aluminate. J Wuhan Univ Technol – Mater Sci Ed 2012;27(2):333–6.
[61] Taylor HFW. Cement Chemistry. London: Taylor & Francis; 2004.
[62] Hong S-Y, Glasser FP. Alkali sorption by C–S–H and C–A–S–H gels: Part II. Role of alumina. Cem Concr Res 2002;32(7):1101–11.
[63] Jackson MD, Logan JM, Scheetz BE, Deocampo DM, Cawood CG, Marra F, et al. Assessment of material characteristics of ancient concretes, Grande Aula, Markets of Trajan, Rome. J Archaeol Sci 2009;36(11):2481–92.
[64] Jackson MD, Vola G, Všianský D, Oleson JP, Scheetz BE, Brandon C, et al. Cement microstructures and durability in ancient Roman seawater concretes. In: Válek J, Hughes JJ, Groot CJWP, editors. Historic Mortars, Characteristics and Tests. Springer-RILEM; 2012. p. 49–76.
[65] Jackson MD, Marra F, Hay RL, Cawood C, Winkler EM. The judicious selection and preservation of tuff and travertine building stone in ancient Rome. Archaeometry 2005;47(3):485–510.
[66] Bentz DP, Irassar EF, Bucher BE, Weiss WJ. Limestone fillers to conserve cement in low w/cm concretes: An analysis based on Powers' model. Concr Intl 2009;31(11):41–6.
[67] Ghrici M, Kenai S, Saidmansour M. Mechanical properties and durability of mortar and concrete containing natural pozzolana and limestone blended cements. Cem Concr Compos 2007;29(7):542–9.